RESEARCH ARTICLE

Check for updates

The missing MIL-101(Mn): geometrically guided synthesis and topologically correlated valence states†

Yonghong Xiao, [ID] [a] Mian Li, [ID] *[a,b] Jian-Rui Chen, [ID] [a] Xin Lian, [ID] [a,c]
Yong-Liang Huang [ID] [d] and Xiao-Chun Huang [ID] *[a,b]

Mixed-valence manganese complexes are of special interest in biocatalysis and magnetism research. Nevertheless, when including manganese clusters into metal–organic frameworks (MOFs), several issues such as valence control, phase selectivity, etc. were usually encountered, hence limiting the discovery of Mn MOFs. The long-sought MIL-101(Mn), a missing piece of the famous MIL-101 (Al, Sc, Ti, V, Cr, Fe) family, has finally been synthesized through a unique, controllable geometrically guided approach, different from the well-developed kinetically modulating approach. It is the first time that the single-crystal structure of a MIL-101 material has been determined by X-ray diffraction. Surprisingly, it is revealed that MIL-101(Mn) exhibits an emergent phenomenon of topologically correlated mixed-valence states, which are characterized by XPS and magnetic measurements. Moreover, the metastable Mn(III) species therein show enzymatic catalytic activity under mild conditions.

Introduction

Metastable trivalent manganese plays a vital role in living systems, especially in many biocatalysts where manganese acts as the active site like Mn_4Ca oxygen-evolving complex (OEC) in photosystem II[1] and some metallocatalases from microbiotics.[2] The widespread presence of manganese in nature has led to the pursuit of various molecular manganese clusters in order to mimic biocatalytic reactions, such as the oxidation of water and other bioactive substrates that are sensitive to the complicated valence and/or spin states of the manganese clusters.[3] In addition, the accessible redox activity allows manganese complexes to be extensively utilized in organic synthesis such as oxidative coupling and cyclization reactions.[4,5] Among

numerous trivalent manganese compounds, manganese carboxylates featuring a trinuclear $[Mn_3O(CH_3COO)_6]$ unit have been extensively studied for magnetism, catalysis and so on.[6,7]

In the context of metal–organic framework (MOF), such a trinuclear $[M_3O(CH_3COO)_6]$ (M = metal) unit can be used as a six-coordinated (6-c) trigonal prismatic building block[8] to build multifarious single/mixed-metal MOF with particular attentions paid to chromium and iron ones.[9–11] Subject to the hard and soft acid and base theory, the synthesis of highly crystalline Cr(III), Mn(III) and Fe(III) MOF materials, especially those with single-crystal quality, is a remaining challenge not fully tackled. Overall, the bond strength follows the order Cr(III) (d^3) > Mn(III) (d^4) > Fe(III) (d^5) combining the factors of increased electrostatic interaction between d-electrons and the hard base ligand[12] and decreased ligand field stabilization energies.[13] Moreover, the ligand (i.e. water) exchange rate of Fe(III) is 10^8 times higher than that of kinetically inert Cr(III),[14] leading to the notorious poor crystallinity and the requirement of high temperature when preparing Cr MOFs. On the other hand, Zhou's group developed a kinetically tuned approach to construct a range of Fe MOFs from pre-assembled Fe(III) trinuclear clusters through ligand exchange.[15] Recently, Wang et al. successfully achieved the conversion from Fe to Cr MOFs with the trigonal prismatic building unit using solvent-assisted metal metastasis.[16] In contrast to the situations of Fe(III) and Cr(III), the problem faced for manganese in forming MOFs is quite different because the metastable Mn(III) has d^4 configuration that can produce Jahn–Teller distortion, which results in

[a]Department of Chemistry and Key Laboratory for Preparation and Application of Ordered Structural Materials of Guangdong Province, Shantou University, Guangdong 515063, China. E-mail: mli@stu.edu.cn, xchuang@stu.edu.cn
[b]Chemistry and Chemical Engineering Guangdong Laboratory, Shantou 515031, China
[c]School of Materials Science and Engineering, National Institute for Advanced Materials, TKL of Metal and Molecule-Based Material Chemistry, Nankai University, Tianjin 300350, China
[d]Department of Medicinal Chemistry, Shantou University Medical College, Shantou, Guangdong 515041, China

†Electronic supplementary information (ESI) available. CCDC 2190013 (for MIL-101(Mn) and 2190014 (for MIL-88B(Mn)-35dmpy). For ESI and crystallographic data in CIF or other electronic format see DOI: https://doi.org/10.1039/d2qi01894b

6124 | Inorg. Chem. Front., 2022, 9, 6124–6132

This journal is © the Partner Organisations 2022

a much greater rate of ligand substitution than that of Cr(III) and Fe(III).[17] Although many trinuclear Mn(II) MOFs were studied on their adsorptive,[18–20] magnetic,[21] and catalytic properties,[22] the synthesis of MOFs with Mn_3O building block containing Mn(III), which might exhibit useful redox-active properties similar to discrete Mn_3O complexes,[23] was rarely reported.[24] Two typical examples are Mn(III)-MIL-100 (**moo** topology) reported in 2013,[25] as well as recently reported mixed-valence Mn(II/III)-MIL-88B (**acs** topology),[26] both of which were built-up through modulating reaction conditions involving *in situ* valence changes of manganese.

Curiously, the synthesis of MIL-101(Mn) (**mtn-e** topology) has not yet been reported till now,[27] despite many other metals (Al, Sc, Ti, V, Cr and Fe) in the MIL-101 family were achieved. This is possibly related to several issues. First, the synthetic difficulty in valence-control and stabilization of Mn(III) may lead to unwanted byproducts with more stable Mn(II) or Mn(IV), which is related to multiple factors such as solvent, temperature, pH values and so on. Secondly, the formation of MIL-101 may face with the competition of a topological isomer (*i.e.* MIL-88B with **acs** topology),[28,29] which is believed to be the thermodynamic product of the reaction.[30] The confluence of above issues distinguish MIL-101(Mn) from MIL-101(Fe or Cr) to be an intricate, unresolved synthetic challenge; that is to say, a unique approach should be developed to stabilize the metastable Mn(III) in the local trinuclear unit and, simultaneously, to isolate the kinetic product of the global networks. Notably, formerly reported methods (modulator,[31] temperature,[30] solvent,[32] type of metal,[33] *etc.*) that worked well for MIL-101 and MIL-88B series with iron or chromium failed for the case of manganese, which will be discussed later in this work. Herein, we present a controllable geometry-guided strategy, accompanied with an *in situ* comproportionation reaction (an initial mixture of low and high Mn oxidation states for the preparation of Mn(III/IV) under mild conditions),[26] for the MIL-101(Mn) synthesis (Scheme 1). Furthermore, we succeeded in obtaining the single-crystal structure of MIL-101 (Mn); in fact, this is the first time that the single-crystal struc-

ture of a MIL-101 material of any metal can be determined by X-ray diffraction.

Results and discussion

To begin with, we noted that MIL-88B and MIL-101 are the thermodynamic and kinetic products of a certain reaction, respectively, on the energetic level.[30] Topologically, MIL-88B belongs to a denser, simpler **acs** net which has only one type of node and edge (*i.e.* with a transitivity of 1 1 2 2).[8] In contrast, the topology of MIL-101, **mtn-e**, has a more complicated structure with large voids, containing 4 types of nodes and 7 types of edges (*i.e.* transitivity 4 7 9 5).[34] Such an observation is in accord with the results from energetic considerations.

There were literatures reporting on the effects of temperature, organic acids, *etc.* on the phase selectivity of MIL series materials.[30,31,33] To examine whether the above-mentioned factors can be considered for obtaining MIL-101(Mn), a series of controlled trials were conducted (see section 3.3 and 3.4 in the ESI†). Firstly, the experiments were carried out from 50 to 80 °C since temperature is normally considered affecting whether the product is thermodynamically or kinetically controlled. According to the final color of the mixture, colorless solution indicated the reduction of high-valence manganese to Mn(II) is more likely to occur over 70 °C, while the reaction is not complete at lower temperature (*e.g.* 50 °C) resulting in deep-brown solution containing Mn(III) (Fig. S4†). Therefore, the change in temperature, although affecting the redox environment, did not contribute to the MIL-101/MIL-88B(Mn) phase selectivity. Some literature emphasized that modulators like benzoic acid can play a phase-selective role in MIL-101 synthesis,[31] but similar trails failed for manganese system (Fig. S5†), because the dilemma of stabilization of trivalent at low temperature and ligand exchange at high temperature are difficult to solve simultaneously. Hence, available strategies are not applicable to MIL-101(Mn) and new synthetic strategies need to be investigated for synthesizing metastable Mn MOFs.
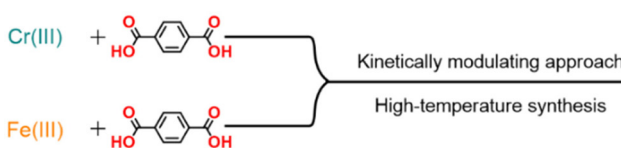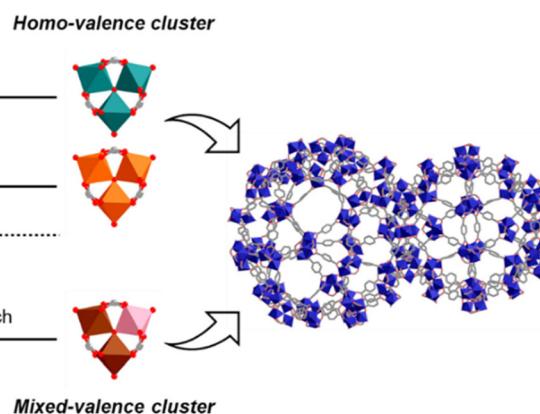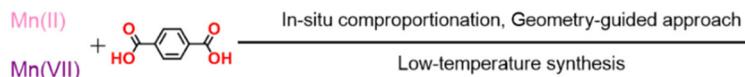
Scheme 1 A representation of the synthesis of MIL-101(Mn) compared with that of classic MIL-101(Fe) and MIL-101(Cr).

Geometrically guided synthesis

Through inspection of the underlying nets, we propose a geometry-guided approach. The connected triangular prisms in the augmented net **acs-a**, the net of MIL-88B, are more regularly arranged (*i.e.* the angles between two edges connecting the prisms are 88.15° and 73.12°). In contrast, the augmented net of MIL-101, **mtn-e-a**, has 4 types of nodes that are more strained when connected (*i.e.* up to 120° between two connecting edges within the six-membered ring, see Fig. S8†). Based on this structural information, we assumed that selective phase tuning of manganese-terephthalate frameworks could be realized by perturbating the coordination geometry of the nodes, and the giant cages with pentagonal and hexagonal windows of MIL-101 structure could allow further steric tuning. MIL-88 has a smaller window size than MIL-101, so introducing bulky terminal ligands on the pore-aperture hinders the formation of MIL-88 and favours MIL-101. To verify the assumption above, pyridine and its derivates, usually found to coordinate in a vertical orientation relative to the planar trinuclear oxo-centered complexes with benzoic acid[35,36] and also used in the synthesis of MIL-88B/D(Cr),[37] are chosen for tuning the crystallization processes under the assumption that they may serve as the geometrical modulators for generating the tension needed in the **mtn-e-a** net of MIL-101. Another rational consideration is pyridine can also work as a weak base for deprotonation of ligand which accelerates the reaction and may lead to a kinetically-favored product.[30]

As shown in Fig. 1a, through progressively increasing the amount of pyridine (see section 3.1 in the ESI†), it was found that the characteristic PXRD peaks at the low angle and around 8–9° started to occur when adding 380 μL of pyridine, which was intensified until the amount of pyridine reached 1400 μL. Eventually dark green powders were obtained when 2 mL pyridine was added, which was confirmed to be pure MIL-101(Mn) octahedral microcrystals with diameters around 200 nm (Fig. S10†). At first glance, the synthesized dark green sample had a color similar to that of the pyridine coordinated trinuclear manganese benzoate complexes, rather than the color of the common cases with coordinated water molecules,[6,36] suggesting pyridine may participate in the construction of MOF structure, which is later confirmed by IR (Fig. S22†) and X-ray photoelectron spectroscopy (XPS) spectra (Fig. S11–14†). After careful adjustment of the synthesis conditions (see section 3.2 in the ESI†), dark green octahedral single crystals of pyridine-modulated MIL-101(Mn) were successfully prepared and the structure was determined by single-crystal X-ray diffraction, in which the introduced pyridine molecules are indeed found to coordinate in a vertical orientation with a part of Mn centers (see Fig. S7,† which will be discussed in detail below). Note that the single-crystal structures of MIL-100/101 type materials (including Cr,[11] Fe[32] and other metals) are generally difficult to obtain.

In order to further demonstrate that the geometry-guided approach for synthesizing MIL-101(Mn) is indeed subject to steric effects, several *para*-substituted pyridine compounds with different steric hindrance were selected for study. The dosage of pyridine derivatives was studied in detail. Considering the alkalinities of pyridine (py), 4-methylpyridine (4-Mepy) and 4-*tert*-butylpyridine (4-*t*Bupy) are quite close (the pK_a of their conjugate acids are 5.2, 6.0 and 6.0, respectively),[38] the contribution of their steric effects to the system can be isolated largely. As a matter of fact, the amount of py, 4-Mepy, and 4-*t*Bupy required to form the pure-phase MIL-101(Mn) decreased sequentially (Fig. 1a–c), which is inversely correlated with the axial length of these three molecules. A detailed analysis on the pore sizes (see section 11.3 in the ESI†) of both MIL-88B and MIL-101 structures gave a clue that such a length-phase relationship may be related to the geometry of the hexagonal channel of MIL-88B. The pyridine derivative molecules cannot coexist in MIL-88B if the axial length of the geometrical modulator is larger than a critical size of 6.36 Å (Fig. S25†), thus tending to generate pyridine-coordinated MIL-101. Based on the results of theoretical calculations (see section 11.1 and 11.2 in the ESI†), the axial length of py (6.53 Å) is slightly larger than the critical size, and this effect is more pronounced for 4-Mepy (7.54 Å) and 4-*t*Bupy (8.66 Å); hence, less amount of geometrical modulator was needed.

Interestingly, among several other trails using pyridine derivatives with large hinderance, 3,5-dimethylpyridine (3,5-dmpy), a non-axially hinderant pyridine derivative, yielded a pure and unreported phase of MIL-88B (Fig. 1d). Unlike the reported MIL-88B(Mn) with space group *Cmcm*,[26] the MIL-88B obtained with 3,5-dmpy (namely MIL-88B(Mn)-35dmpy) crystallized in a trigonal space group (*P$\bar{3}$1c*) which is also different from other reported solvated MIL-88B that has higher symmetrical six-fold symmetry.[10,39] The coordinated 3,5-dmpy molecules are compatibly aligned in the channel due to size matching and hydrophobic interactions existed between the methyl groups (Fig. 1e). Besides, an *ortho*-disubstituted pyridine, 2,6-dimethylpyridine did not play a phase selective role even with a large dosage (Fig. S6†) due to the greater hinderance unfit to the coordination site. These results indicate that it is the *para*-substituted pyridines that are preferable for solving the difficult phase selectivity problem in synthesizing the missing piece, *i.e.* MIL-101(Mn).

Topologically correlated valence state

When analyzing the single-crystal structure of the pyridine-supported MIL-101(Mn) (see section 4.1 in the ESI†), we realized that cooperativity exists between the local Mn(II/III) mixed-valency in the trinuclear [Mn$_3$O(CH$_3$COO)$_6$] unit and the global requirement of 4 types of crystallographically independent trinuclear units in the underlying **mtn-e** net, which gives rise to an emergent phenomenon of topologically correlated valence states. In order to clarify this observation, we performed a detailed investigation of previously reported structures, including discrete [Mn$_3$O(CH$_3$COO)$_6$] clusters and MOFs with such a secondary building unit (SBU). As depicted in Fig. 2 (left), it is informative to classify the structural characteristics of the trinuclear clusters according to the Mn–μ_3O bond

6126 | *Inorg. Chem. Front.*, 2022, **9**, 6124–6132

This journal is © the Partner Organisations 2022
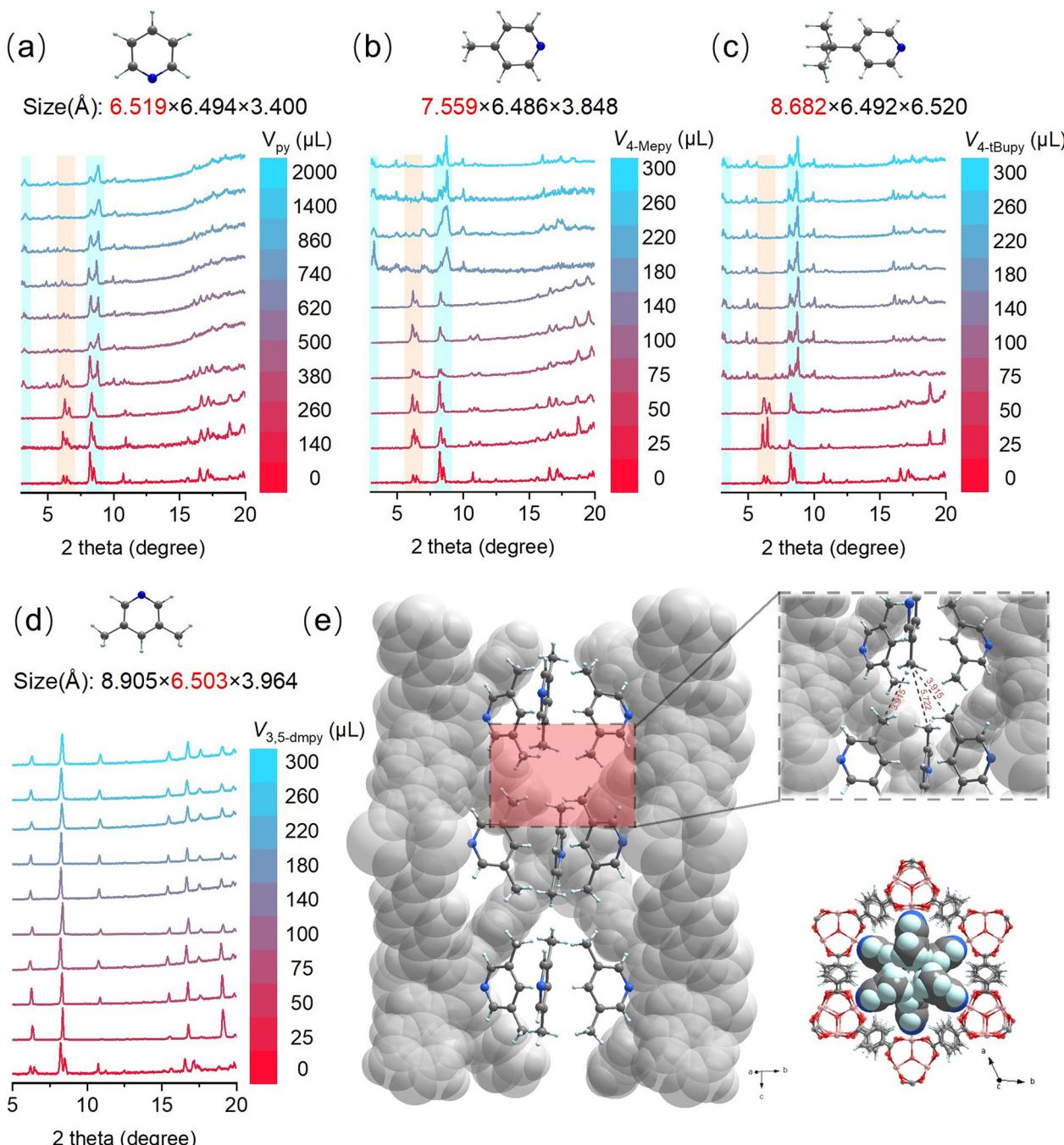
Fig. 1 Geometry-guided synthesis of MIL-101(Mn) through introducing geometrical modulators such as (a) pyridine, (b) 4-methylpyridine, (c) 4-tertbutylpyridine and (d) 3,5-dimethylpyridine, tested by PXRD. (e) Overall and detailed structure of the unexpected MIL-88B(Mn) phase, showing the channel alone c-axis. Note that the red and blue regions highlighted in (a)–(c) correspond to the characteristic peaks of MIL-88B(Mn) and MIL-101(Mn) phases, respectively.

length data,[40] which can be divided into three regions (highlighted in yellow, blue, and red cycles). For most reported discrete trinuclear clusters, the valence of Mn ions is either pure trivalent or mixed trivalent-divalent in 2 to 1 ratio from every aspect.[40] The ones with three Mn(III) have equal Mn^{III}–μ_3O bond lengths (ranging from 1.88–1.90 Å) for each case, lying on the yellow zone. Most of the mixed-valence Mn_3O clusters,

with $d_2(Mn^{II}$–$\mu_3O)$ longer than $d_1(Mn^{III}$–$\mu_3O)$, fall in the blue region covering a wide distribution, which is related to the push–pull electronic effect of the ligands and the crystal packing effects. The most special cases, within the red zone, are a few mixed-valence clusters with apparently equal d_1 and d_2 that are slightly longer than normal Mn^{III}–μ_3O bond lengths, which is believed to be enforced by the crystal sym-

This journal is © the Partner Organisations 2022

Inorg. Chem. Front., 2022, **9**, 6124–6132 | **6127**
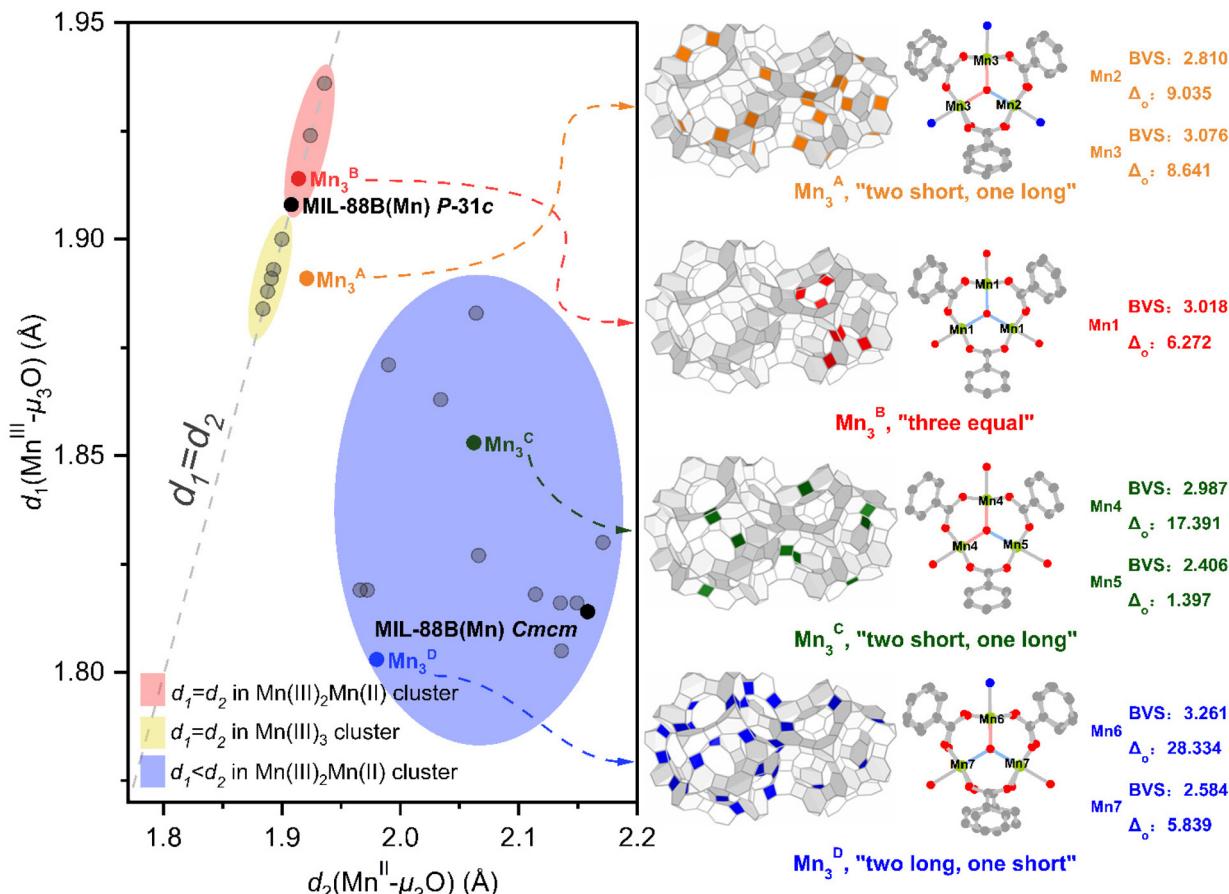
**Fig. 2** Topologically correlated valence states in MIL-101(Mn) in the context of wide-ranging bond length distribution of Mn–μ_3O extracted from various discrete and networked (*i.e.* in MOFs) clusters. In the left part, the bond length data are divided into three (yellow, blue, and red) regions; the gray dots are from discrete clusters (data from ref. 40) while the black and colored dots are from MOFs. In the right part, several structural indicators, including correlated locations in **mtn-e-a** net, bond-valence sum (BVS) calculations and distortion factors (Δ_o), of the four types of clusters in MIL-101(Mn) are given.

metry; in such a case the valence of Mn should be further characterized, *e.g.* by magnetic measurements.[41]

Under the context above, we wish to disclose the issues brought up by the Mn(II/III) mixed valency in networked [Mn$_3$O (CH$_3$COO)$_6$] clusters (*i.e.* in MOFs). Let us first consider the simpler cases of MIL-88B(Mn) which have only one crystallographically independent [Mn$_3$O(CH$_3$COO)$_6$] cluster. In the reported structure of MIL-88B(Mn) which crystalized in *Cmcm* space group,[26] it was reasoned that the unequal Mn^{II}–μ_3O and Mn^{III}–μ_3O bond lengths in the mixed-valence [Mn$_3$O (CH$_3$COO)$_6$] cluster had broken the crystal symmetry from hexagonal (that of the intrinsic symmetry of **acs** net, *P6$_3$/mmc*) to orthorhombic. Therefore, its Mn–μ_3O bond length indicator lies in the blue area (Fig. 2, left), which we consider to be a normal case of mixed-valence states in networked systems. As for the MIL-88B(Mn)-35dmpy phase isolated in this work, which crystallized in *P$\bar{3}$1c* space group, the open Mn sites, as well as the voids of the MOF, are fully occupied by the neutral 3,5-dmpy molecules (see Fig. 1e, bottom right); therefore, the valences of manganese should be +3 and +2 in 2 : 1 ratio in

order to maintain the overall electrical neutrality. However, it is found that the Mn^{II}–μ_3O and Mn^{III}–μ_3O bond lengths are equal, *i.e.* d_2(Mn^{II}–μ_3O) = d_1(Mn^{III}–μ_3O) = 1.91 Å, which falls in the red region and is close to the Mn^{III}–μ_3O bond lengths. On the other hand, there is a mixed-valence MIL-88B(Mn)-tpt phase supported by a tritopic linker, 2,4,6-tri(4-pyridyl)-1,3,5-triazine (*i.e.* tpt), which crystallized in the ideal-symmetry *P6$_3$/mmc* space group, and in which and the Mn–μ_3O bond lengths are found to be equally 2.10 Å, close to the Mn^{II}–μ_3O bond lengths.[42] These two extreme cases suggest that the Mn(II/III) valence states in MIL-88B(Mn) analogues are correlated topologically and further imposed by the three-fold symmetry of the crystal, and thus the Mn^{II}–μ_3O and Mn^{III}–μ_3O bond lengths are not necessarily unequal.

On the basis of the unusual observations from MIL-88B (Mn) series discussed above, one can expect MIL-101(Mn), which crystallized in the intrinsic symmetry of **mtn-e** net (*Fd$\bar{3}$m*) and has four types of crystallographically independent trinuclear clusters, should experience unpredictable (so-called emergent) topologically correlated valence states. This is

6128 | *Inorg. Chem. Front.*, 2022, **9**, 6124–6132

This journal is © the Partner Organisations 2022

because the four types of nodes are enforced by different local symmetries in the network, and the occurrence of geometrical frustration[35] for trinuclear mixed-valence manganese clusters brings further complication. As shown in Fig. 2 (right), we denote the four types of clusters Mn_3^X (X = A, B, C, or D). It is found that the pyridine modulators, all perpendicular with the Mn_3O plane due to steric hinderance of the neighboring benzoate groups,[6] only coordinate with parts of the open Mn sites —for Mn_3^A, the solvent molecules ligated to the cluster are all pyridine, while the coordinated solvent molecules in Mn_3^D exhibit inhomogeneity, consisting of two water (or DMF) and one pyridine molecule. Note that Mn_3^A is located at the midpoint of the edge shared by the three pentagons, while Mn_3^D is located at the intersection of two five-membered rings and one six-membered ring (Fig. S8†). This coordination imbalance makes Mn_3^D subject to distinct local environment where the pyridine geometrical modulator plays the key role for the formation of MIL-101 phase instead of the geometrically more regular MIL-88B. When comparing Mn_3^B and Mn_3^C in which the coordinated solvent molecules are all water (or DMF), it is noted that Mn_3^B exhibits equal $Mn-\mu_3O$ bond lengths due to the local three-fold symmetry, and thus belongs to the red region. In fact, the four Mn_3^X nodes (in the ratio A : B : C : D = 6 : 2 : 3 : 6) fall within different regions marked in Fig. 2 (left).

When looking into the $Mn-\mu_3O$ bond length data in MIL-101(Mn) (see Table S2 in the ESI†), we noted that the four Mn_3^X clusters exhibit different characteristics, i.e. Mn_3^A "two short, one long" (1.9142 Å, 1.9227 Å), Mn_3^B "three equal" (1.9175 Å), Mn_3^C "two short, one long" (1.8732 Å, 2.0340 Å), and Mn_3^D "two long, one short" (1.9803 Å, 1.8071 Å), respectively. We further calculated the secondary geometric indicators, bond-valence sum (BVS)[1,43,44] and octahedron distortion factor (Δ_o),[45] the later indicating the Jahn–Teller distortion of Mn(III) (see Fig. 2, right). From these analyses, it is found that Mn_3^C belongs to the normal case of mixed-valence states (in the blue region), that is, Mn(III) : Mn(II) = 2 : 1, with Mn4 showing a typical $Mn^{III}-\mu_3O$ bond length and a significant octahedron distortion ($\Delta_o \sim 17.391$). Note that Mn_3^C locates in separated positions of the **mtn-e-a** net (green trigonal prisms in Fig. 2, right). In stark contrast, Mn_3^D resides in a higher hierarchy of hexagonal six-membered ring (blue trigonal prisms in Fig. 2, see also Fig. S10†), in which Mn6 has the shortest Mn(III)–μ_3O bond length and the greatest $\Delta_o \sim 28.334$, and thus the Mn(III) : Mn(II) ratio in Mn_3^D is unusually 1 : 2. Most notably, Mn_3^A and Mn_3^B (orange and red trigonal prisms, respectively, in Fig. 2) are highly correlated, forming a higher order of "triangles surrounding a tetrahedron" (see Fig. S9†). Although the $Mn-\mu_3O$ bond lengths in Mn_3^A and Mn_3^B are all close to those of Mn(III), in order to maintain the overall charge balance there must be Mn(II) existing which, however, cannot be distinguished explicitly. Note that the BVS and Δ_o indicators for Mn_3^A and Mn_3^B are also very close in value, suggesting the mixed-valence states within them are numerically averaged for the bond lengths and angles, due to the strongly correlated "triangles surrounding a tetrahedron" geometry. Moreover, we are aware of the existence of spin frustra-

tion for μ_3O-centered trinuclear mixed-valence manganese clusters;[35] a further implication is the famous triangular and tetrahedral frustration models of antiferromagnetically interacting spins[46] that are integrated in the "triangles surrounding a tetrahedron" arrangement. These are geometrical prerequisites for the exotic properties, such as valence-bond condensation, in frustrated magnets.[47,48]

The mixed-valence states in MIL-101(Mn) was also characterized by magnetic and spectroscopic techniques. XPS was conducted to probe the valence of manganese ions within the clusters. Compared with those of divalent and trivalent manganese acetates, the XPS for MIL-101(Mn) shows differences of binding energy (ΔE) in Mn 3s area (Fig. S13†), lying between 6.1 eV (for Mn^{2+}) and 5.4 eV (for Mn^{3+}). Further investigation of 2p area (Fig. 3a) shows significant satellite shake-up signals of 2p1/2 and 2p3/2 for Mn(II) at 656.6 eV and 645.7 eV, respectively, indicating the existence of mixed-valence manganese ions. The magnetic property of MIL-101(Mn) were characterized using a SQUID magnetometer. As shown in Fig. 3b, the dc magnetic susceptibility data were collected at a magnetic field of 5000 Oe in various temperature from 1.8 K to 300 K. At 300 K, a slightly lower experimental $\chi_M T$ value (around 8.52 cm³·K mol⁻¹) was recorded in comparison with a theoretical value (10.375 cm³·K mol⁻¹ when $g = 2$, $S_{Mn(II)} = 5/2$, $S_{Mn(III)} = 2$) for a high-spin $Mn^{II}Mn_2^{III}$ system with no interaction. The $\chi_M T$ decreases with decreasing temperature, indicating the nature of overall weak antiferromagnetic coupling interaction, which provides an explanation for the situation that the $\chi_M T$ is smaller than the theoretical value at 300 K. Another possible reason is the presence of other spin states. At 2 K, the experimental value of $\chi_M T$ is 1.82 cm³·K mol⁻¹, close to 1.875 cm³·K mol⁻¹ for a ground state $S = 3/2$. The experimental plot of $1/\chi_M T$ vs. T in the range of 150–300 K can be well fitted to the Curie–Weiss law with a Curie constant $C = 11.13$ cm³ mol⁻¹ K and a large and negative Weiss constant $\theta = -91.45$ K (Fig. S19†), which confirms the antiferromagnetic coupling of Mn in this temperature range.

Furthermore, the magnetic susceptibility data for MIL-101 (Mn) are simulated using spin Hamiltonian in PHI (Fig. 3b, see section 8.3 in the ESI†).[49] The optimal fitting results gave J and J' values of −14.9(1) and ~0 cm⁻¹, describing the isotropic
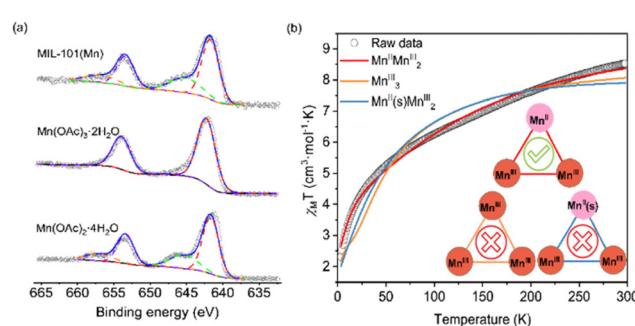

Fig. 3 Mixed-valence state characterizations of MIL-101(Mn) by (a) XPS and (b) temperature-dependent magnetic susceptibility measurements.

exchange interactions of Mn(III)–Mn(III) and Mn(II)–Mn(III), respectively. This result is similar to the mixed-valence Mn-MIL-88B-Me4 phase reported in the literature.[26] The isotropic g-value of divalent and trivalent manganese is 2 and 1.93, identical to those in MIL-88B series. However, the axial zero-field splitting parameter D is 4.4(1) and −1.3(2) cm$^{−1}$ for Mn(II) and Mn(III), respectively, indicating a distortion of the coordination configuration.[26] All the above evidences indicate the trinuclear mixed-valence manganese clusters in MIL-101(Mn) is in the form of Mn^{II}Mn$_2^{III}$ in average. Other simulation results, such as Mn$_3^{III}$ and Mn^{II}(s)Mn$_2^{III}$ (s stands for strong field), can be ruled out due to poor fitting. The possibility of emergent properties in frustrated magnets requires the use of more advanced characterization techniques and/or theoretical insights to confirm.[47,48]

Biomimic catalytic activity of metastable species

Many peroxidases in nature contain multinuclear manganese clusters, and the mechanism of their catalysis is mostly due to the valence change of manganese in the carboxylic acid bridge during catalytic hydrogen peroxide decomposition.[50] The large window of the MIL-101(Mn) structure, its porosity (see section 14 in the ESI†), and the metallocatalases-like mixed-valence manganese sites prompted us to investigate its enzymatic catalytic properties. The catalytic properties of MIL-101(Mn) were tested by using 3,3′,5,5′-tetramethylbenzidine (TMB) as a chromogenic prober frequently used for photometric determination of peroxidase activity (Fig. 4a, detailed experimental procedures see section 15 in the ESI†).[50] At room temperature,

the introduction of 0.5 mL MOF suspension resulted in a distinct blue color of tetramethylbenzidine solution, which turned yellow after acidification (Fig. 4b and c), implying the generation of benzidine radicals and the peroxidase-like oxidizing ability of MIL-101(Mn), which is temperature and catalyst dosage dependent (Fig. 4d and e). Unfortunately, the material decomposed after testing due to the aqueous catalytic environment, but it still has an organocatalytic potential in organic phase, like manganese acetate, a commercial catalyst with catalytic oxidation activity,[7] which deserve to be further explored.

Conclusions

In conclusion, the present work uncovers a missing piece of the puzzle, i.e. the metastable, mixed-valence manganese phase belonging to the MIL-101 family. Synthetically demanding MIL-101(Mn) has been successfully prepared through a unique, controllable approach, i.e. geometrically guided synthesis by modulating pyridyl modulators. The single crystal structure of MIL-101(Mn) has been directly determined through X-ray diffraction, which reveals the emergent topologically correlated valence states that could serve as a platform of frustrated magnets in future studies. The oxidase-like catalytic activity of MIL-101(Mn) has been confirmed, paving the way for bio-applications of redox-active Mn MOFs.

Author contributions

Yonghong Xiao carried out the synthetic experiments, characterization, data analysis and manuscript writing. Jian-Rui Chen performed the gas adsorption test. Xin Lian performed the theoretical calculation. Yong-Liang Huang performed the SC-XRD structure refinement. Xiao-Chun Huang and Mian Li supervised the work and edited the manuscript.

Conflicts of interest

There are no conflicts to declare.
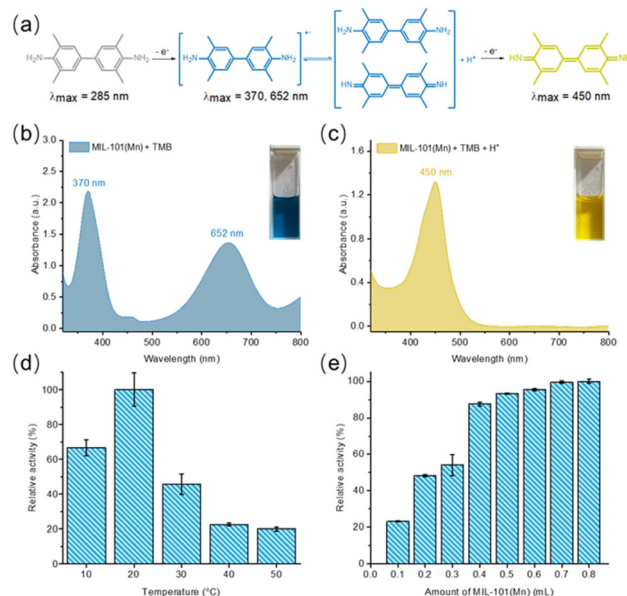
Fig. 4 Enzymatic catalytic properties of MIL-101(Mn). (a) Schematic illustration of peroxidase activity determination by TMB oxidation reaction monitored via UV-Vis test. Characteristic (b) blue colored radical cation and (c) yellowish imine are observed during catalysis. Reactivity is related to (d) temperature and (e) catalyst dosage.

References

1 C. Zhang, C. Chen, H. Dong, J.-R. Shen, H. Dau and J. Zhao, A synthetic Mn$_4$Ca-cluster mimicking the oxygen-evolving center of photosynthesis, *Science*, 2015, **348**, 690–693.

2 J. W. de Boer, W. R. Browne, B. L. Feringa and R. Hage, Carboxylate-bridged dinuclear manganese systems – from catalases to oxidation catalysis, *C. R. Chim.*, 2007, **10**, 341–354.

3 M. M. Najafpour, G. Renger, M. Hołyńska, A. N. Moghaddam, E. M. Aro, R. Carpentier, H. Nishihara, J. J. Eaton-Rye, J. R. Shen and S. I. Allakhverdiev, Manganese compounds as water-oxidizing catalysts: from the natural water-oxidizing complex to nanosized manganese oxide structures, *Chem. Rev.*, 2016, **116**, 2886–2936.

4 B. Ramesh, C. R. Reddy, G. R. Kumar and B. V. S. Reddy, Mn(OAc)$_3$*2H$_2$O promoted addition of arylboronic acids to quinoxalin-2-ones, *Tetrahedron Lett.*, 2018, **59**, 628–631.

5 W. E. Fristad and J. R. Peterson, Manganese(III)-mediated γ-lactone annulation, *J. Org. Chem.*, 1985, **50**, 10–18.

6 J. Ribas, B. Albela, H. Stoeckli-Evans and G. Christou, Synthesis and magnetic properties of six new trinuclear oxo-centered manganese complexes of general formula [Mn$_3$O(X-benzoato)$_6$L$_3$] (X=2-F, 2-Cl, 2-Br, 3-F, 3-Cl, 3-Br; L=pyridine or water) and crystal structures of the 2-F, 3-Cl, and 3-Br complexes, *Inorg. Chem.*, 1997, **36**, 2352–2360.

7 M. Mondal and U. Bora, Recent advances in manganese(III) acetate mediated organic synthesis, *RSC Adv.*, 2013, **3**, 18716–18754.

8 M. Li, D. Li, M. O'Keeffe and O. M. Yaghi, Topological analysis of metal–organic frameworks with polytopic linkers and/or multiple building units and the minimal transitivity principle, *Chem. Rev.*, 2014, **114**, 1343–1370.

9 P. Horcajada, H. Chevreau, D. Heurtaux, F. Benyettou, F. Salles, T. Devic, A. Garcia-Marquez, C. Yu, H. Lavrard, C. L. Dutson, E. Magnier, G. Maurin, E. Elkaïm and C. Serre, Extended and functionalized porous iron(III) tri- or dicarboxylates with MIL-100/101 topologies, *Chem. Commun.*, 2014, **50**, 6872–6874.

10 C. Serre, C. Mellot-Draznieks, S. Surblé, N. Audebrand, Y. Filinchuk and G. Férey, Role of solvent-host interactions that lead to very large swelling of hybrid frameworks, *Science*, 2007, **315**, 1828–1831.

11 G. Férey, C. Mellot-Draznieks, C. Serre, F. Millange, J. Dutour, S. Surblé and I. Margiolaki, A chromium terephthalate-based solid with unusually large pore volumes and surface area, *Science*, 2005, **309**, 2040–2042.

12 I. D. Brown and R. D. Shannon, Empirical bond-strength–bond-length curves for oxides, *Acta Crystallogr., Sect. A: Cryst. Phys., Diffr., Theor. Gen. Crystallogr.*, 1973, **29**, 266–282.

13 D. A. Johnson and P. G. Nelson, Ligand field stabilization energies of the hexaaqua 3+ complexes of the first transition series, *Inorg. Chem.*, 1999, **38**, 4949–4955.

14 L. Helm and A. E. Merbach, Inorganic and bioinorganic solvent exchange mechanisms, *Chem. Rev.*, 2005, **105**, 1923–1959.

15 D. Feng, K. Wang, Z. Wei, Y.-P. Chen, C. M. Simon, R. K. Arvapally, R. L. Martin, M. Bosch, T.-F. Liu, S. Fordham, D. Yuan, M. A. Omary, M. Haranczyk, B. Smit and H.-C. Zhou, Kinetically tuned dimensional augmentation as a versatile synthetic route towards robust metal-organic frameworks, *Nat. Commun.*, 2014, **5**, 5723.

16 J.-H. Wang, Y. Zhang, M. Li, S. Yan, D. Li and X.-M. Zhang, Solvent-assisted metal metathesis: a highly efficient and versatile route towards synthetically demanding chromium metal–organic frameworks, *Angew. Chem., Int. Ed.*, 2017, **56**, 6478–6482.

17 C. Philouze, M. Henry, N. Auger, D. Vignier, M. Lance, M. Nierlich and J. J. Girerd, Experimental and theoretical investigations of condensation and disproportionation of Mn(bpy)Cl$_3$(H$_2$O) in aqueous solution, *Inorg. Chem.*, 1999, **38**, 4–11.

18 J. Jia, F. Sun, T. Borjigin, H. Ren, T. Zhang, Z. Bian, L. Gao and G. Zhu, Highly porous and robust ionic MOFs with nia topology constructed by connecting an octahedral ligand and a trigonal prismatic metal cluster, *Chem. Commun.*, 2012, **48**, 6010–6012.

19 Q.-G. Zhai, X. Bu, C. Mao, X. Zhao, L. Daemen, Y. Cheng, A. J. Ramirez-Cuesta and P. Feng, An ultra-tunable platform for molecular engineering of high-performance crystalline porous materials, *Nat. Commun.*, 2016, **7**, 13645.

20 Y.-C. He, J. Yang, W.-Q. Kan, H.-M. Zhang, Y.-Y. Liu and J.-F. Ma, A new microporous anionic metal–organic framework as a platform for highly selective adsorption and separation of organic dyes, *J. Mater. Chem. A*, 2015, **3**, 1675–1681.

21 M. Di, J. Shen, Z. Cui, X. Zhang and J. Zhang, Assembly of metal-organic frameworks based on 4-connected 3,3′,5,5′-azobenzenetetracarboxylic acid: structures, magnetic properties, and sensing of Fe3+ ions, *New J. Chem.*, 2019, **2**, 4226–4234.

22 Q. Liu, H. Cong and H. Deng, Deciphering the spatial arrangement of metals and correlation to reactivity in multivariate metal-organic frameworks, *J. Am. Chem. Soc.*, 2016, **138**, 13822–13825.

23 R. G. Pearson, Absolute electronegativity and hardness: application to inorganic chemistry, *Inorg. Chem.*, 1988, **27**, 734–740.

24 E. F. Chernova, A. S. Ovsyannikov, S. E. Solovieva, I. S. Antipin, N. Kyritsakas, M. W. Hosseini and S. Ferlay, Control of dimensionality in Manganese Coordination Polymers using rigid tetrahedral-shaped [1.1.1.1]metacyclophane ligands bearing benzoate coordinating sites: from homochiral 1D to 3D diamond-like structures, *Inorg. Chem. Commun.*, 2019, **106**, 197–201.

25 H. Reinsch and N. Stock, Formation and characterisation of Mn-MIL-100, *CrystEngComm*, 2013, **15**, 544–550.

26 M. R. Mian, U. Afrin, M. S. Fataftah, K. B. Idrees, T. Islamoglu, D. E. Freedman and O. K. Farha, Control of the porosity in manganese trimer-based metal-organic frameworks by linker functionalization, *Inorg. Chem.*, 2020, **59**, 8444–8450.

This journal is © the Partner Organisations 2022

Inorg. Chem. Front., 2022, **9**, 6124–6132 | **6131**

27 M. Y. Zorainy, M. Gar Alalm, S. Kaliaguine and D. C. Boffito, Revisiting the MIL-101 metal-organic framework: design, synthesis, modifications, advances, and recent applications, *J. Mater. Chem. A*, 2021, **9**, 22159–22217.

28 K. Kersten, R. Kaur and A. Matzger, Survey and analysis of crystal polymorphism in organic structures, *IUCrJ*, 2018, **5**, 124–129.

29 D. Bara, C. Wilson, M. Mörtel, M. M. Khusniyarov, S. Ling, B. Slater, S. Sproules and R. S. Forgan, Kinetic control of interpenetration in Fe-biphenyl-4,4′-dicarboxylate metal-organic frameworks by coordination and oxidation modulation, *J. Am. Chem. Soc.*, 2020, **141**, 8346–8357.

30 F. Carson, J. Su, A. E. Platero-Prats, W. Wan, Y. Yun, L. Samain and X. Zou, Framework isomerism in vanadium metal-organic frameworks: MIL-88B(V) and MIL-101(V), *Cryst. Growth Des.*, 2013, **13**, 5036–5044.

31 L. Yang, T. Zhao, I. Boldog, C. Janiak, X. Y. Yang, Q. Li, Y. J. Zhou, Y. Xia, D. W. Lai and Y. J. Liu, Benzoic acid as a selector-modulator in the synthesis of MIL-88B(Cr) and nano-MIL-101(Cr), *Dalton Trans.*, 2019, **48**, 989–996.

32 S. Bauer, C. Serre, T. Devic, P. Horcajada, J. Marrot, G. Férey and N. Stock, High-throughput assisted rationalization of the formation of metal organic frameworks in the iron(III) aminoterephthalate solvothermal system, *Inorg. Chem.*, 2008, **47**, 7568–7576.

33 L. Pukdeejorhor, K. Adpakpang, P. Ponchai, S. Wannapaiboon, S. Ittisanronnachai, M. Ogawa, S. Horike and S. Bureekaew, Polymorphism of mixed metal Cr/Fe terephthalate metal-organic frameworks utilizing a microwave synthetic method, *Cryst. Growth Des.*, 2019, **19**, 5581–5591.

34 M. O'Keeffe, M. A. Peskov, S. J. Ramsden and O. M. Yaghi, The Reticular Chemistry Structure Resource (RCSR) database of, and symbols for, crystal nets, *Acc. Chem. Res.*, 2008, **41**, 1782–1789.

35 J. K. McCusker, H. G. Jang, S. Wang, G. Christou and D. N. Hendrickson, Ground-state variability in μ_3-oxide trinuclear mixed-valence manganese complexes: spin frustration, *Inorg. Chem.*, 1992, **31**, 1874–1880.

36 A. D. Zarlaha, P. G. Koutsoukos, C. Skordilis and P. J. Pomonis, Preparation and characterization of manganese oxidic mesoporous particles obtained via the trinuclear $[Mn_3O(CH_3COO)_6(pyr)_3]ClO_4$ complex, *J. Colloid Interface Sci.*, 1998, **202**, 301–312.

37 S. Surblé, C. Serre, C. Mellot-Draznieks, F. Millange and G. Férey, A new isoreticular class of metal-organic-frameworks with the MIL-88 topology, *Chem. Commun.*, 2006, 284–286.

38 Y. Yan, E. L. Zeitler, J. Gu, Y. Hu and A. B. Bocarsly, Electrochemistry of aqueous pyridinium: exploration of a key aspect of electrocatalytic reduction of CO_2 to methanol, *J. Am. Chem. Soc.*, 2013, **135**, 14020–14023.

39 C. Serre, F. Millange, S. Surblé and G. Férey, A route to the synthesis of trivalent transition-metal porous carboxylates with trimeric secondary building units, *Angew. Chem., Int. Ed.*, 2004, **43**, 6285–6289.

40 S. G. Baca, H. Stoeckli-Evans, C. Ambrus, S. T. Malinovskii, I. Malaestean, N. Gerbeleu and S. Decurtins, Synthesis, crystal structures and magnetic properties of trinuclear oxo-centered homo- and mixed-valence manganese pivalate complexes with imidazole (Im) and 1-methylimidazole (1-MeIm): $[Mn^{III}_3O(O_2CCMe_3)_6(Im)_3]$ $(Me_3CCO_2) \cdot 0.5Me_3CCO_2H$ and $[Mn^{III}_2Mn^{II}O(O_2CCMe_3)_6$ $(1\text{-MeIm})_3]$, *Polyhedron*, 2006, **25**, 3617–3627.

41 T. C. Stamatatos, D. Foguet-Albiol, S. C. Lee, C. C. Stoumpos, C. P. Raptopoulou, A. Terzis, W. Wernsdorfer, S. O. Hill, S. P. Perlepes and G. Christou, "Switching on" the properties of single-molecule magnetism in triangular manganese(III) complexes, *J. Am. Chem. Soc.*, 2007, **129**, 9484–9499.

42 T. Zhang, J. W. Cao, Y. F. Dai, H. Feng, S. Y. Zhang, J. Chen, T. Wang, Y. Wang and K. J. Chen, Charge-state control of a host metal-organic framework enabled by axially co-ordinated tripyridine ligand alternation, *Cryst. Growth Des.*, 2022, **22**, 3594–3600.

43 G. J. Palenik, Bond valence sums in coordination chemistry using oxidation state independent R_0 values, *Inorg. Chem.*, 1997, **36**, 4888–4890.

44 I. D. Brown and D. Altermatt, Bond-valence parameters obtained from a systematic analysis of the Inorganic Crystal Structure Database, *Acta Crystallogr., Sect. B: Struct. Sci.*, 1985, **41**, 244–247.

45 F. K. Chiang, M. W. Chu, F. C. Chou, H. T. Jeng, H. S. Sheu, F. R. Chen and C. H. Chen, Effect of Jahn-Teller distortion on magnetic ordering in $Dy(Fe,Mn)O_3$ perovskites, *Phys. Rev. B: Condens. Matter Mater. Phys.*, 2011, **83**, 10–13.

46 L. Balents, Spin liquids in frustrated magnets, *Nature*, 2010, **464**, 199–208.

47 J. P. Sheckelton, J. R. Neilson, D. G. Soltan and T. M. McQueen, Possible valence-bond condensation in the frustrated cluster magnet $LiZn_2Mo_3O_8$, *Nat. Mater.*, 2012, **11**, 493–496.

48 M. L. Baker, G. A. Timco, S. Piligkos, J. S. Mathieson, H. Mutka, F. Tuna, P. Kozłowski, M. Antkowiak, T. Guidi, T. Gupta, H. Rath, R. J. Woolfson, G. Kamieniarz, R. G. Pritchard, H. Weihe, L. Cronin, G. Rajaraman, D. Collison, E. J. L. McInnes and R. E. P. Winpenny, A classification of spin frustration in molecular magnets from a physical study of large odd-numbered-metal, odd electron rings, *Proc. Natl. Acad. Sci. U. S. A.*, 2012, **109**, 19113–19118.

49 N. F. Chilton, R. P. Anderson, L. D. Turner, A. Soncini and K. S. Murray, PHI: A powerful new program for the analysis of anisotropic monomeric and exchange-coupled polynuclear *d*- and *f*-block complexes, *J. Comput. Chem.*, 2013, **34**, 1164–1175.

50 A. J. Wu, J. E. Penner-Hahn and V. L. Pecoraro, Structural, spectroscopic, and reactivity models for the manganese catalases, *Chem. Rev.*, 2004, **104**, 903–938.